The *Escherichia coli* F_OF_1 γM23K Uncoupling Mutant Has a Higher $K_{0.5}$ for P_i. Transition State Analysis of This Mutant and Others Reveals That Synthesis and Hydrolysis Utilize the Same Kinetic Pathway

Marwan K. Al-Shawi, Christian J. Ketchum, and Robert K. Nakamoto*

Department of Molecular Physiology and Biological Physics, University of Virginia, Charlottesville, Virginia 22906-0011

Received June 20, 1997; Revised Manuscript Received August 19, 1997[⊗]

ABSTRACT: The *Escherichia coli* F_OF_1 ATP synthase uncoupling mutation, γM23K, was found to increase the energy of interaction between γ and β subunits, prevent the proper utilization of binding energy to drive catalysis, and block the enzyme in a P_i release mode. In this paper, the effects of this mutation on substrate binding in cooperative ATP synthesis are assessed. Activation of ATP synthesis by ADP and P_i was determined for the γM23K F_OF_1. The $K_{0.5}$ for ADP was not affected, but $K_{0.5}$ for P_i was approximately 7-fold higher even though the apparent V_{max} was close to the wild-type level. Wild-type enzyme had a turnover number of 82 s^{-1} at pH 7.5 and 30 °C. During oxidative phosphorylation, the apparent dissociation constant (K_I) for ATP was not affected and was 5−6 mM for both wild-type and γM23K enzymes. Thus, the apparent binding affinity for ATP in the presence of $\Delta\mu_H+$ was lowered by 7 orders of magnitude from the affinity measured at the high-affinity catalytic site. Arrhenius analysis of ATP synthesis for the γM23K F_OF_1 revealed that, like those of ATP hydrolysis, the transition state $\Delta H^{\ddagger}$ was much more positive and $T\Delta S^{\ddagger}$ was much less negative, adding up to little change in $\Delta G^{\ddagger}$. These results suggested that ATP synthesis is inefficient because of an extra bond between γ and β subunits which must be broken to achieve the transition state. Analysis of the transition state structures using isokinetic plots demonstrate that ATP hydrolysis and synthesis utilize the same kinetic pathway. Incorporating this information into a model for rotational catalysis suggests that at saturating substrate concentrations, the rate-limiting step for hydrolysis and synthesis is the rotational power stroke where each of the β subunits changes conformation and affinity for nucleotide.

The F_OF_1[1] ATP synthase complex contains at least eight different subunits divided into two sectors. The membranous F_O carries out H^+ transport and in *Escherichia coli* has three subunits in a stoichiometry of $ab_2c_{\sim 10}$. The transport is energetically coupled to catalytic sites in the soluble F_1, which has five different subunits, $\alpha_3\beta_3\gamma\delta\epsilon$. In recent years, much insight into the mechanism of coupling has been obtained from extensive mutagenic, biochemical, and biophysical analyses (for reviews, see refs 1−6) and from the generation of high-resolution structural information (i.e., refs 7−10). From this work, it has become clear that the F_OF_1 complex uses conformational linkages to modulate the kinetics and thermodynamics of one function by another. In normal functioning during conditions of ATP synthesis, imposition of a $\Delta\mu_H+$ causes an increase in the binding rate constant and affinity for P_i (*11*−*14*), an increase in the off-rate constant for ATP (*13, 15*), and an increase in the rate of the catalytic step (*11*). It is not surprising, therefore, that perturbations (amino acid substitutions, protein labeling, or inhibitor binding) in what are believed to be the transport or coupling domains influence thermodynamic parameters of catalysis. For example, Matsuno-Yagi and Hatefi (*16*) and Penefsky (*17*) showed that oligomycin or dicyclohexylcarbodiimide (DCCD), inhibitors which bind or react with F_O, alter the ATP binding properties of F_1. Recently, we found that the uncoupling mutation, γM23K, caused altered transition state thermodynamic parameters of ATP hydrolysis (see below; ref 18). There is little doubt that ATP synthase functions are linked so that a perturbation that affects one function must have an effect on the other functions (*19*).

With this premise in mind, we take advantage of the uncoupling mutation γM23K. Previously, we reported that this mutation perturbed coupling efficiency between transport and catalysis (*20*). We further demonstrated that γM23K caused altered interactions between subunits β and γ (*18*). On the basis of the X-ray crystallographic structure of Abrahams *et al.* (*7*), as well as site-directed mutagenic analysis (*20*), the guanidinium or ϵ-amino group from Arg or Lys would likely form an ionized hydrogen bond with the carboxylate of β-Glu381 of the highly conserved β^{380}-DELSEED^{386} loop. Thermodynamic analysis of the ATPase reaction of the γM23K enzyme and suppressor mutations were consistent with this suggestion (*18*; C. J. Ketchum, M. K. Al-Shawi, and R. K. Nakamoto, unpublished results). This led to the conclusion that γM23K is an added-function mutation that increases the energy of interaction between γ and β subunits through the formation of an additional hydrogen bond.

† This work was supported by PHS grants GM50957 to R.K.N. and GM52502 to M.K.S. C.J.K. is a recipient of a NIH predoctoral grant HL07284.

* Please address correspondence to Department of Molecular Physiology and Biological Physics, University of Virginia, P.O. Box 10011, Charlottesville, VA 22906-0011. Tel: (804) 982-0279. Fax: (804) 982-1616. E-mail: rkn3c@virginia.edu.

⊗ Abstract published in *Advance ACS Abstracts,* October 1, 1997.

[1] Abbreviations: CCCP, carbonyl cyanide-*m*-chlorophenylhydrazone; DCCD, *N,N*′-dicyclohexylcarbodiimide; F_1, the soluble portion of the F_OF_1 ATP synthase; F_OF_1, the complete ATP synthase complex; TES, *N*-tris(hydroxylmethyl)methyl-2-aminoethanesulfonic acid.

S0006-2960(97)01478-5 CCC: $14.00

If this interpretation is correct, then certain predictions can be made regarding the nature of ATP synthesis by the uncoupling mutation γM23K. Amongst the most important are the following: (1) changes in substrate binding energy utilization by the mutant enzyme; (2) little or no change in the chemical and overall cooperative mechanism of ATP synthesis in the mutant enzyme; (3) uncoupling of H^+ transport from catalysis is due to the creation of a branched pathway that occasionally bypasses the coupling step. In the preceding paper in this issue (*21*), we presented evidence that showed the validity of the first prediction: the mutation perturbs the ability of the enzyme to use binding energy to achieve the optimal substrate coordination necessary to carry out the chemistry of synthesis.

In this paper, we study kinetic and thermodynamic parameters of ATP synthesis under cooperative (multisite) catalytic modes in order to test the other two predictions and to assess how the mutation affects the transmission of coupling information during steady state ATP synthesis. To do this, we introduce new quantitative assays for analysis and understanding of coupling mutations. Additionally, we provide new information regarding the rate-limiting step of ATP synthesis and hydrolysis and further draw general conclusions regarding the nature of energy coupling by F_OF_1 ATP synthases.

EXPERIMENTAL PROCEDURES

Strains and Isolation of Membranes. Membranous F_OF_1 was obtained from strain KF10rA harboring derivatives of low copy number plasmid pBWG15 (*22*). Membranes were prepared as described previously (*23*). Determination of F_1 content in *E. coli* membranes was performed by quantitative immunoblot analysis and comparing results with known amounts of purified F_1 as described previously (*18*).

General Methods and Materials. Protein concentrations were determined by the method of Lowry *et al.* (*24*). Formation of an electrochemical gradient of protons ($\Delta\mu_H+$) was measured by 1 μM acridine orange fluorescence quenching in the buffers and conditions used for ATP synthesis. Technical details were previously described in Nakamoto *et al.* (*25*). ATP hydrolysis measured by production of P_i was assayed as previous described (*18*). NADH-driven respiration rates were measured polargraphically with an Instrumentation Laboratories Clark oxygen electrode in a thermostated reaction vessel. Oxygen concentrations were from Lessler and Brierley (*26*). Concentrations of ionic species of Mg, P_i, and nucleotides were determined by the algorithm of Fabiato and Fabiato (*27*). Pyruvate kinase was from Boehringer Mannheim and hexokinase (H-4502) was from Sigma. [^{32}P]P_i (PBS13A) and [γ-^{32}P]ATP (PB10132) were from Amersham. All other reagents were of the highest available quality.

Determination of Kinetic Constants for ATP Synthesis. NADH-driven ATP synthesis was measured in the presence of a hexokinase trap by modification of the method of Wise and Senior (*28*). For determination of kinetic constants as a function of P_i, the reaction medium contained 25 mM TES-KOH, 200 mM KCl, 5 mM $MgSO_4$, 10 mM glucose, 1 mM ADP, and 0.1−12 mM [^{32}P]P_i, pH adjusted to 7.5 at 30 °C. To control for ionic and chaotropic effects, experiments were also performed in which the total added anion was kept constant at 12 mM by replacing P_i with SO_4^{2-} as needed. Just prior to the experiment, 50 units/mL of hexokinase was added and 2 mL of buffer was removed to a 16 × 100 mm glass tube in a reciprocating water bath. Freshly thawed *E. coli* membranes (0.2−0.6 mg) were added and incubated with vigorous shaking for 2 min, at which time ATP synthesis was started by the addition of 2 mM NADH. At 30−60 s time intervals, 0.42 mL samples were removed and vortexed with 80 μL of ice-cold 1.5 M $HClO_4$. Total ATP synthesis rates were determined (*28*) and each experiment was performed at least in triplicate. ATP synthesis rates were linear for several minutes (>4 min). For each incubation, a control experiment was done in the presence of 5 μM CCCP to determine the background phosphorylation rates which were subtracted from the total rate to obtain the oxidative phosphorylation rate. Fractional background phosphorylation decreased as the concentration of [^{32}P]P_i increased from 0.1 to 12 mM as well as being a function of the particular membrane preparation used (data not shown). The range of background phosphorylation here was 7−42% of total phosphorylation. For determination of kinetic constants as a function of ADP, experiments were done essentially as given above with the following modifications. The buffer contained 25 mM TES-KOH, 200 mM KCl, 5 mM $MgSO_4$, 10 mM glucose, and 10 mM [^{32}P]P_i, pH 7.5. In order to keep the free Mg^{2+} and P_i ionic species relatively constant, supplemental Mg^{2+} was added with ADP in the constant molar ratio of 0.76 Mg/ADP. ADP concentration was varied from 50 nM to 10 mM. For determination of the apparent inhibitory constant (K_I) of ATP on oxidative phosphorylation, experiments were performed as above with 1 mM ADP and 10 mM [^{32}P]P_i, but without any hexokinase. ATP synthesis was started by the addition of 2 mM NADH supplemented with 0−20 mM Mg/ATP (1:1 constant molar ratio) in the experimental buffer above. After acid quenching as above, [γ-^{32}P]ATP formation was determined by the method of Sugino and Miyoshi (*29*). ATP synthesis rates were linear for >4 min at all ATP concentrations used. Control experiments demonstrated that, in the absence of added ATP, the initial rate of [γ-^{32}P]ATP formation was the same as the glucose-6-^{32}P formation rate in the presence of a hexokinase trap.

Arrhenius Analysis and Derivation of Transition State Thermodynamic Parameters. Activation energies and entropic and enthalpic components of the transition state for multisite ATP hydrolysis were calculated from measurements of maximal rates of ATPase activities as a function of temperature as detailed in Al-Shawi *et al.* (*18*). For ATP synthesis, the thermodynamic parameters were determined in a two step process. (1) E_a and $\Delta H^{\ddagger}$ were calculated from plots of log velocity versus the reciprocal temperature (calculations detailed in Al-Shawi and Senior, ref 30). ATP synthesis was measured as a function of temperature, essentially as described in the previous section. The buffer contained 25 mM TES-KOH, 200 mM KCl, 5 mM $MgSO_4$, 10 mM glucose, 1 mM ADP, 10 mM [^{32}P]P_i, and 50 units/mL hexokinase, pH adjusted to 7.5 at each required temperature. Synthesis was started by the addition of 2 mM NADH. To ensure that valid parameters were being measured, preliminary experiments were done over a wide temperature range from which it was established that linear Arrhenius relationships existed over the temperature range of 20−30 °C for the enzymes studied. (2) To calculate $\Delta G^{\ddagger}$ and $T\Delta S^{\ddagger}$ as previously described (*30*), turnover numbers

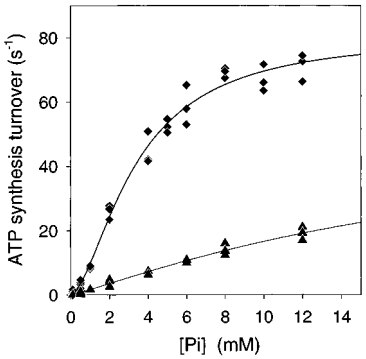

FIGURE 1: Oxidative phosphorylation as a function of P_i concentration. The membranous F_OF_1 ATP synthesis turnover is plotted against P_i concentration. Turnover numbers were calculated by dividing the velocity by the actual F_OF_1 content of the membranes as determined by quantitative immunoblot analysis (*18*). Experiments were done at pH 7.5, 30 °C and the concentration of MgADP was 0.72−0.78 mM (see Experimental Procedures for further details). The solid lines were derived by fitting the data to the Hill equation of cooperativity. (◆) Wild-type F_OF_1; parameters of fit, $V_{max} = 80$ s^{-1}, n_H (Hill coefficient) = 1.6, $K_{0.5} = 3.3$ mM, $r = 0.995$. (▲) γM23K F_OF_1; parameters of fit, $V_{max} = 58$ s^{-1}, $n_H = 1.1$, $K_{0.5} = 22$ mM, $r = 0.987$.

(k_{cat}) were calculated from the measured V_{max} for ATP synthesis as determined in the previous paragraph and adjusted for the experimentally determined F_1 content of membranes. Verification of isokinetic relationships were carried out by the methods of Exner (*31*).

RESULTS

Effects of the γM23K Mutation on ATP Synthesis. To study the effects of the γM23K mutation on ATP synthesis, steady state kinetic parameters of cooperative "multisite" ATP synthesis were measured. Figure 1 shows the ATP synthesis rate as a function of the concentration of P_i in the presence of saturating ADP. Because of the ever increasing background from the ^{32}P isotope, the titration had to be limited to 12 mM P_i and saturation could not be reached for the γM23K enzyme. Nevertheless, the data points could be readily fit by the Hill equation for cooperativity. From these plots, the apparent $K_{0.5}$ for P_i (constant for half maximal activation by P_i) was derived and found to be increased in γM23K F_OF_1 relative to wild-type F_OF_1. Thus $K_{0.5}$ for P_i changes from 3.5 mM for wild-type to 23 mM for γM23K F_OF_1 (Figure 1 and Table 1) and is consistent with the enhanced P_i off-rate measured for γM23K F_1 in unisite analysis (see preceding paper in this issue, ref 21). The $K_{0.5}$ for P_i for wild-type F_OF_1 determined above was similar to the K_M for P_i of 2.5 mM for GTP synthesis by wild-type F_OF_1 previously determined under similar conditions by Wise and Senior (*28*) and in reasonable agreement with the value of K_M for P_i for ATP synthesis of 0.7 ± 0.2 mM determined under different experimental conditions by Fischer et al. (*14*). V_{max} values when converted to turnover numbers are quite similar for both enzymes and were 82 and 60 s^{-1} for wild-type and γM23K F_OF_1, respectively (Table 2). At this point, it is instructive to recall that the effects of the γM23K mutation are not just kinetic in nature, but also affect the thermodynamic coupling efficiency. This is most easily seen by the impaired ability of γM23K F_OF_1 to pump protons and generate a $\Delta\mu_H+$ (*20*).

An interesting feature of Figure 1 is the apparent cooperativity of P_i activation of ATP synthesis in wild-type F_OF_1. The apparent average Hill coefficient for activation of ATP synthesis by P_i was 1.6 (Table 1). Such a phenomenon was not seen with the other substrate for ATP synthesis, namely ADP (Figure 2 and Table 1). Furthermore, the results shown in Figure 1 did not change when SO_4^{2-} was added in conjunction and as a replacement for P_i such that the total oxyanion added was 12 mM (results not shown). Thus, ionic strength changes were unlikely to be the cause of the apparent cooperativity. Whether this result indicates an absolute requirement for phosphate binding to two different catalytic sites to allow ATP synthesis is currently unknown and will require further investigation. Notwithstanding the above, the reduction in apparent P_i cooperativity by γM23K F_OF_1 (Hill coefficient, $n_H = 1.1$, Table 1) implies that this phenomenon is a manifestation of normal coupled cooperative ATP synthesis.

MgADP activation of ATP synthesis followed normal Michaelis−Menton kinetics with K_M values of 39 and 26 μM for wild-type and γM23K F_OF_1, respectively (Figure 2 and Table 1) and are similar to the values obtained previously for normal F_OF_1 (*14*, *28*). Thus, ADP binding during ATP synthesis did not appear to be affected by the γM23K mutation. Because the dependence of ATP synthesis on the substrates P_i and ADP were not linear functions of concentration but rather hyperbolic functions (Figures 1 and 2), it can be concluded that the calculated turnover rates for the enzymes at saturating P_i and ADP (Table 2) correspond to a kinetic step after the binding of P_i and ADP.

We measured the back inhibition of ATP synthesis by added external ATP to investigate the effect of the γM23K mutation on the ATP release and binding site during turnover. The apparent ATP inhibition constant of oxidative phosphorylation was similar for wild-type and γM23K membranes and was 4.7 and 5.8 mM, respectively (Table 1). This result implies that the γM23K mutation had little effect on the site of ATP release and binding during multisite catalysis. Additionally, these results indicate that under conditions of

Table 1: Average Steady State Kinetic Parameters of ATP Synthesis at 30 °C and pH 7.5[a]

	P_i values			ADP values[b]			
preparation	V_{max}[c] (μmol/min/mg)	$K_{0.5}$[d] (mM)	n_H[e]	V_{max}[f] (μmol/min/mg)	$K_{0.5}$[d] (μM)	n_H[e]	inhibition by ATP, K_I[g] (mM)
WT membranes	0.15	3.5	1.6	0.13 (0.16)[h]	39	1.0	4.7
γLys-23 membranes	0.095	23	1.1	0.027 (0.094)[h]	26	1.0	5.8

[a] See Experimental Procedures for assay conditions. [b] Values are presented for MgADP. [c] V_{max} values for P_i at saturating ADP concentrations. In this table, activities are presented per milligram of total membrane protein. [d] $K_{0.5}$ is the concentration of substrate required for half-maximal activity. [e] n_H is the apparent Hill coefficient for the substrate. [f] For technical reasons measurements of ATP synthesis as a function of ADP concentration could not be determined at saturating P_i concentrations but was determined at 10 mM P_i. Thus, V represents the maximal velocity at 10 mM P_i. [g] K_I is the apparent ATP inhibition constant of oxidative phosphorylation. [h] Values in parentheses represent the calculated true V_{max} at saturating P_i concentrations utilizing the activity (V) measured at 10 mM P_i and correcting for saturating P_i using the kinetic parameters of ATP synthesis at saturating ADP and varying P_i given in this table.

Table 2: Transition State Thermodynamic Parameters at 30 °C and pH 7.5 for ATP Synthesis and Hydrolysis by Membranous F_OF_1 Preparations and Comparison between Wild-Type and γM23K Enzymes

preparation	reaction direction	turnover number[a] (s^{-1})	Q_{10} values[b]	$\Delta H^{\ddagger}$	$\Delta\Delta H^{\ddagger c}$	$T\Delta S^{\ddagger}$ (kJ/mol)	$\Delta(T\Delta S)^{\ddagger c}$	$\Delta G^{\ddagger}$	$\Delta\Delta G^{\ddagger c}$
WT membranes	synthesis	82	2.3	58		−4.8		63	
γLys-23 membranes	synthesis	60	9.3	162	104	98	103	64	0.8
WT membranes[d]	hydrolysis	425	1.6	31		−28		59	
γLys-23 membranes[d]	hydrolysis	92	2.9	77	46	14	42	63	3.9

[a] See Experimental Procedures for assay conditions. Turnover numbers were calculated by correcting the measured true V_{max} activities by the actual F_oF_1 content of the membranes as determined by quantitative Western blot analysis (see Al-Shawi *et al.*, ref 18 for details). [b] Q_{10} values represent the reaction rate at 30 °C divided by the corresponding rate at 20 °C. In the presence of the uncoupler CCCP, oxidation of NADH by the respiratory chain had a Q_{10} value of 2.0 under these experimental conditions. See main text footnote two. [c] $\Delta\Delta$ values are differences between parameters for mutant γM23K enzyme and the corresponding wild-type enzyme. [d] Values for ATP hydrolysis were taken from Al-Shawi *et al.* (*18*).

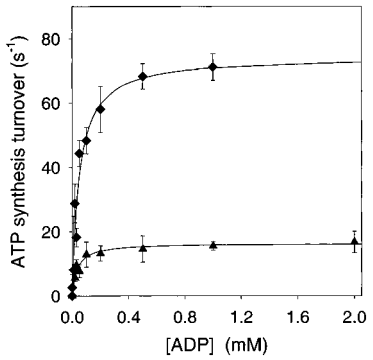

FIGURE 2: Oxidative phosphorylation as a function of ADP concentration. The membranous F_OF_1 ATP synthesis turnover is plotted against the ADP concentration. Experiments were done at pH 7.5, 30 °C, and 10 mM [^{32}P]P_i (see Experimental Procedures for further details). Results are shown with standard deviations, and the solid lines were derived by fitting the entire data sets to the Michaelis−Menton equation. (◆) Wild-type F_OF_1; parameters of fit, $V_{max} = 74\ s^{-1}$, $K_M = 38\ \mu M$, $r = 0.982$. (▲) γM23K F_OF_1; parameters of fit, $V_{max} = 16\ s^{-1}$, $K_M = 26\ \mu M$, $r = 0.877$.

oxidative phosphorylation (large $\Delta\mu_H+$), the dissociation constant for ATP in *E. coli* was in the millimolar range as has recently been demonstrated for bovine mitochondrial F_OF_1 (*15*). The 7 orders of magnitude drop ($\Delta G = 41.5$ kJ/mol) in apparent affinity for MgATP in the presence of $\Delta\mu_H+$ from that measured at the "unisite" (*21*) is in the range expected for a binding change mechanism (*32*). To allow for any ATP-P_i exchange that might be occurring, two types of control experiments were performed. (1) Using the experimental conditions above, F_OF_1-driven ATP synthesis was measured by adding 0−10 mM Mg/ATP (1:1) in the absence of added NADH. It was found that there was no significant incorporation of [^{32}P]P_i into ATP with or without CCCP. This was not surprising given the unfavorable conditions for ATP hydrolysis and the intrinsic proton leakiness of the membranes. (2) ATP hydrolysis was assayed in the presence of NADH by adding 0−10 mM [γ-^{32}P]Mg/ATP (1:1) with 2 mM NADH at the start and measuring production of [^{32}P]P_i as a function of time. It was found that after an initial burst of ATP hydrolysis there was zero ATPase activity under steady state conditions when $\Delta\mu_H+$ was fully established. This was in contrast to the linear rates of ATP synthesis under identical experimental conditions. From these two control experiments, it can be concluded that ATP-P_i exchange did not affect our results in any way. In summary, we found that the γM23K mutation did not affect the sites of ADP binding and ATP release during ATP synthesis, but did affect the apparent affinity and cooperativity of P_i binding which has been suggested to be a coupling step in the transmission of $\Delta\mu_H+$ energy into chemical conformational energy (*11*).

Recently, Etzold *et al.* (*33*) have published turnover numbers for ATP synthesis by wild-type *E. coli* F_OF_1 which were somewhat higher than the value found in the present study (270 s^{-1} versus 141 s^{-1} for 37 °C). This difference can be attributed to an underestimation of the true active fraction of F_OF_1 present. These authors utilized residual ATP hydrolysis after DCCD inhibition as an indication of the active fraction present. They subtracted a substantial background rate of 10% of total ATPase, which was DCCD insensitive from the small residual ATPase rate after DCCD inhibition. Experimentally, DCCD does not fully inactivate *E. coli* membrane F_OF_1 ATPase activity (e.g., ref 34) and *E. coli* strains not expressing functional F_OF_1 have very little membrane ATPase activity (e.g., ref 35). In contrast, we make no active site corrections in this study and assume that all the F_OF_1 that we quantify experimentally is fully active in ATP synthesis and hydrolysis.

Altered Transition State Thermodynamic Parameters of ATP Synthesis in the γM23K Mutant Enzyme. We previously measured the thermodynamic parameters of the transition state of ATP hydrolysis by Arrhenius analysis of steady state turnover (*18*). Here, we extend this analysis to the synthesis of ATP with the aim to determine if the same transition state structures and thermodynamic impairment mechanisms were operating in both directions of turnover. Membranes containing wild-type or γM23K F_OF_1 had linear Arrhenius plots for ATP synthesis from 20 to 30 °C (Figure 3); however, above 30 °C, the plots became nonlinear and the activity decreased (Figure 3). Additionally, the temperature for maximal activity varied from preparation to preparation (average was 33 ± 2 °C). This last effect was thought to be due to the variation of intrinsic proton leakiness of the membranes, which is expected to increase as a function of temperature (*33*). Over the linear range, the Q_{10} values for ATP synthesis were 2.3 and 9.3 for wild-type and γM23K F_OF_1, respectively (Table 2), indicating a large difference in thermodynamic parameters of ATP synthesis. For comparison, the Q_{10} value for uncoupled NADH oxidation was 2.0 (Table 2), which is clearly different from the values above.[2]

Control experiments were performed within the "linear" temperature range to establish the validity of the measured

[2] This value is included for comparison purposes only because the Q_{10} value for NADH oxidation does not represent a single reaction. Normal *E. coli* membranes contain two membrane-bound NADH dehydrogenases and two terminal ubiquinol oxidases (oxygen reductases); the relative amounts of these enzymes depends on growth conditions (*57*).

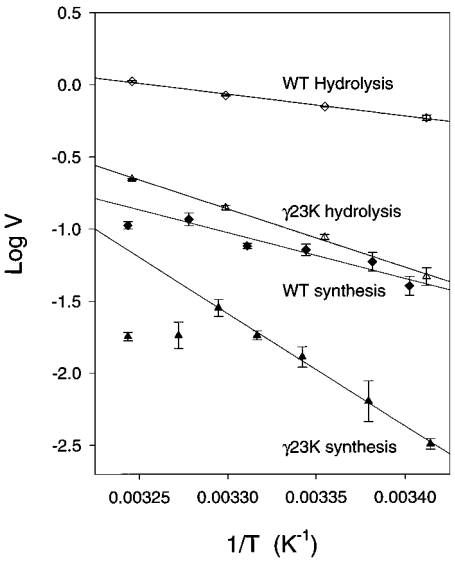

FIGURE 3: Arrhenius analysis of ATP synthesis and hydrolysis by wild-type and γM23K F_OF_1. Log *V* (maximal velocity in micromoles per microgram per minute) is plotted against the reciprocal of absolute temperature. ATP synthesis and ATPase activities were assayed from 20 to 35 °C as detailed in Experimental Procedures. Each point is the average of at least three experiments with the standard deviation indicated. The lines plotted were generated by linear least-squares regression of the individual experimental points. Wild-type F_OF_1 ATP hydrolysis (◇; $r = 0.993$) and synthesis (◆; $r = 0.925$). γM23K F_OF_1 ATP hydrolysis (△; $r = 0.992$) and synthesis (▲; $r = 0.981$).

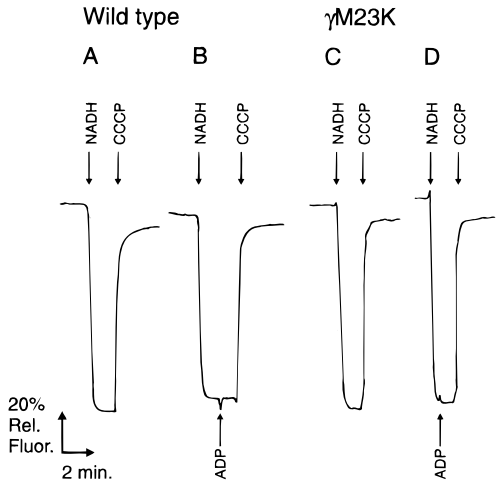

FIGURE 4: Formation of an electrochemical gradient of protons by NADH oxidation. Under experimental conditions of ATP synthesis, acridine orange fluorescence quenching was monitored at 530 nm with excitation at 460 nm. Traces A and C (wild-type and γM23K, respectively) show the steady state $\Delta\mu_H+$ during oxidative phosphorylation; 0.4 mg of membrane vesicle protein was suspended in 2 mL of a buffer containing 25 mM TES-KOH, 200 mM KCl, 5 mM $MgSO_4$, 10 mM glucose, 1 mM ADP, 10 mM KP_i, and 1 μM acridine orange at pH 7.5, 25 °C, with vigorous mixing. Proton pumping was started by the addition of 2 mM NADH. CCCP (5 μM) was added to end the reaction and to establish the 100% fluorescence value. Traces B and D (wild-type and γM23K, respectively) show the changes in $\Delta\mu_H+$ on initiation of oxidative phosphorylation; 0.4 mg of membrane vesicle protein were suspended in 2 mL of a buffer similar to the one above but lacking ADP. After a steady state $\Delta\mu_H+$ was established by NADH oxidation, oxidative phosphorylation was initiated by the addition of 0.3 mM buffered ADP (0.76 molar ratio of Mg/ADP; see Experimental Procedures for further details).

parameters. (1) To measure $\Delta\mu_H+$ qualitatively by fluorescence quenching, 1 μM acridine orange was added to the ATP synthesis buffers. On initiation of NADH oxidation in the presence of 1 mM ADP, a large acridine orange quenching effect was seen for both wild-type and γM23K membranes (Figure 4, traces A and C). The extent of the quenching was similar to that seen when no ADP was present (Figure 4, traces B and D). Furthermore, the initiation of phosphorylation by the addition of 0.3 mM ADP did not cause a drop in the extent of quenching (Figure 4, traces B and D), indicating that $\Delta\mu_H+$ remained unchanged. (2) Using an oxygen electrode under the experimental conditions of ATP synthesis in the linear Arrhenius range, it was found that the membranes exhibited respiratory control when oxidative phosphorylation was initiated with ADP pulses as above such that state 3 respiration (oxidative phosphorylation rate) was faster than state 4 respiration (basal oxidative rate) in all cases (rate enhancement around 1.1-fold; data not shown). Furthermore, the addition of 5 μM CCCP further increased the rate of respiration beyond the maximum rate seen in state 3 (rate enhancement 1.1−1.4-fold; data not shown).[3] These controls indicated that the $\Delta\mu_H+$ generated and respiratory capacity were not rate limiting in our experiments and, further, that the large NADH respiratory capacity of the *E. coli* KF10rA membranes could overcome the large intrinsic leakiness in the "linear" temperature range employed.

From the Arrhenius data, we calculated the enthalpic, entropic, and free energy terms for the transition states of ATP synthesis and hydrolysis for the wild-type and γM23K F_OF_1 at 30 °C (Table 2). For both ATP synthesis and ATP hydrolysis, the γM23K F_OF_1 relative to wild-type F_OF_1 had a much more positive $\Delta H^‡$ and much less negative $T(\Delta S^‡)$ which together add up to a small difference in $\Delta G^‡$. As mentioned in the introductory portion of this paper, these results suggested that the mutation caused the formation of additional bonds within the enzyme that must be broken in order to achieve the transition state. The new ATP synthesis results reinforced the suggestion that γM23K is an added function mutation that increases the energy of interaction between γ and β subunits by formation of an ionized hydrogen bond between γM23K and one of the βGlu381 residues (*18*).

Verification of Isokinetic Relationships. For a given reaction series that uses the same transition state there should be a quantitative relationship between enthalpy and entropy of activation such as an isokinetic relationship (*31*). This relationship is given by eq 1:

$$\Delta H^‡ = h_o^‡ + \beta\Delta S^‡ \quad (1)$$

where β is the isokinetic temperature and $h_o^‡$ is the intrinsic enthalpy of the transition state (model enthalpy). This relationship can also be written in terms of entropy as

[3] The calculated P/O ratios (ATP synthesized/O consumed) were ≤0.55; however, this value is not very informative since *E. coli* membranes as isolated are intrinsically leaky to protons (*33*). The leak leads to low P/O ratios because a significant portion of the respiratory protons are short circuited (*58*). Furthermore, the two NADH dehydrogenases and two terminal oxidases each pump differing numbers of protons such that the expected P/O ratio from NADH oxidation is not constant but depends on the particular membrane preparation employed (*57*).

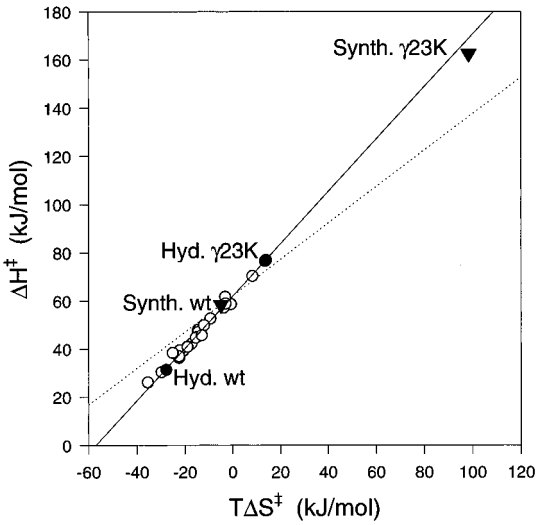

FIGURE 5: Isokinetic plot of ATP synthesis and hydrolysis by F_OF_1 preparations containing various mutations. The enthalpic term, $\Delta H^{\ddagger}$ of activation for k_{cat}, is plotted against the entropic term, $T\Delta S^{\ddagger}$, at 30 °C. (▼) Thermodynamic parameters for ATP synthesis determined in this study. (○) Thermodynamic parameters for ATP hydrolysis by various wild-type, and γ and β subunit mutant membranous F_OF_1 preparations determined previously (*18*). The solid line shows the linear least-squares regression of the data for coupled hydrolysis of ATP by F_OF_1 preparations (gradient = 1.086; β = 56.0 °C; $h_o^{\ddagger}$ = 61.9 kJ/mol; $Ts_o^{\ddagger}$ = −57.0 kJ/mol; r = 0.995). For comparison the dotted line shows the linear regression for uncoupled hydrolysis by wild-type, bovine mitochondrial, γ and β subunit mutant soluble F_1 preparations determined previously (*18*). For the sake of clarity, experimental points for soluble F_1 are not shown (gradient = 0.755; β = −44.1 °C; $h_o^{\ddagger}$ = 62.1 kJ/mol; $Ts_o^{\ddagger}$ = −82.2 kJ/mol; r = 0.992).

follows:

$$\Delta S^{\ddagger} = s_o^{\ddagger} + \Delta H^{\ddagger}/\beta \qquad (2)$$

where $s_o^{\ddagger}$ is the intrinsic entropy of the transition state (model entropy).

In order to show that the same transition state was being measured in coupled ATP synthesis as coupled ATP hydrolysis, we constructed isokinetic plots of $\Delta H^{\ddagger}$ versus $T\Delta S^{\ddagger}$ (Figure 5), which graphically illustrate the effects of a series of mutations on the structure of the transition state. Because the value of β does not depend on the direction in which the reaction is written (*31*), we can compare the results of ATP synthesis directly with the results of ATP hydrolysis. It was found that the results of coupled ATP synthesis fell on, and were, a continuum of the regression line formed by coupled ATP hydrolysis by F_OF_1 preparations of widely diverse origins. This is strong evidence, shown for the first time, that cooperative ATP synthesis and hydrolysis utilize the same transition state structures, and therefore, synthesis and hydrolysis utilize the same kinetic pathway. As previously discussed in this paper, the rate-limiting step in ATP synthesis for which the transition state was measured was not the step of ADP nor P_i binding. Similarly for coupled ATP hydrolysis, because the dependence of velocity was a hyperbolic function of ATP concentration (results not shown), the transition state being measured at V_{max} was not referable to the ATP binding step. Thus, the transition state of Figure 5 was unlikely to be a binding or release step but, as discussed later, is thought to be due to a rotational coupling step.

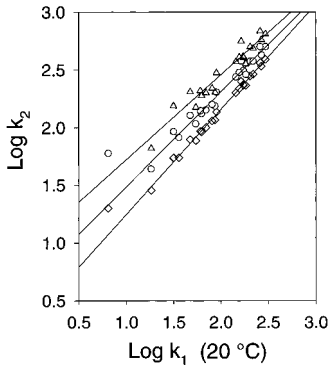

FIGURE 6: Isokinetic correlations. Log k_2 (log of k_{cat} at three different temperatures) is plotted against log k_1 (log of k_{cat} at 20 °C) for the membranous F_OF_1 preparations of Figure 5 during ATP hydrolysis or synthesis. The solid lines were obtained by linear regression analysis; 25 °C (◇; r = 0.967); 30 °C (○; r = 0.987); 35 °C (△; r = 0.967). See Results for further details.

To verify the isokinetic relationship described above, we used the methods recommended by Exner (*31*; see also ref 36 for a recent enzymological example of the application of the methods utilized). In isokinetic relationships, there is a linear free energy relationship between two rate constants (k_1 and k_2) measured at two temperatures ($T_2 > T_1$), which can be given by eq 3 (*31*):

$$\log k_2 = a + b \log k_1 \qquad (3)$$

where a and b are constants. Such functions were plotted for the experimental rate constants measured for the enzymes shown in Figure 5. Figure 6 shows that there were excellent linear correlations between the experimental rate constants derived at three different temperatures (25, 30, and 35 °C) compared to the rate constants determined at 20 °C, thus confirming the relationship shown in Figure 5.

Additional verification for the isokinetic relationship was obtained by statistical analysis of the experimental Arrhenius plots for all the enzyme preparations (see ref 31 for details). By the nonparametric statistical methods of Cornish-Bowden (*37*), β was calculated from the Arrhenius data to be 57 °C, which was in excellent agreement with the value of 56 °C determined in Figure 5. Thus, we can conclude that the same transition state was being measured in coupled ATP synthesis as was in coupled ATP hydrolysis.

DISCUSSION

In this paper, we employed kinetic and thermodynamic analyses that are new in the study of the steady-state ATP synthesis properties of mutant enzymes. This approach proved to be particularly revealing with respect to understanding the mechanism of energy coupling. We took advantage of the uncoupling mutation, γM23K, which was previously found to cause large increases in $\Delta H^{\ddagger}$ and $\Delta S^{\ddagger}$ parameters of the transition state of steady state ATP hydrolysis. These results suggested an extra hydrogen-bond interaction formed between γ and β subunits (*18*). In the case of steady state ATP synthesis, the increases of $\Delta H^{\ddagger}$ and $\Delta S^{\ddagger}$ were even larger (Table 2), indicating that the effects of the γM23K mutation are more severe in the direction of coupled ATP synthesis than in the direction of coupled ATP hydrolysis. From the results of Figure 5, it can be concluded that cooperative ATP synthesis and hydrolysis utilize the same transition state structures, and therefore, synthesis and

hydrolysis utilize the same kinetic pathway. This would mechanistically explain the thermodynamic control by $\Delta\mu_H+$ of the direction of flux (ATP synthesis or hydrolysis) in *E. coli*.

Figure 5 also shows that the coupled transition state structure for ATP synthesis and hydrolysis by membranous F_OF_1 preparations was clearly different from the transition state structure for uncoupled ATP hydrolysis by soluble F_1 preparations. This is indicated by the different slopes of soluble F_1 [dashed line, individual data points are seen in Figure 8 of Al-Shawi *et al*. (*18*) versus membranous F_OF_1 (solid line). A trivial explanation for this observation would be that the two lines were referring to different chemical steps (transition states). This explanation is unlikely in view of the fact that the two lines intersect at the intrinsic enthalpy values of the transition states ($h_o^‡$ values were 61.9 and 62.1 kJ/mol for the coupled transition state and the uncoupled transition state, respectively). At the point of intersection where $T\Delta S^‡ = 0$, $\Delta G^‡$ and $\Delta H^‡$ for both reaction series are the same; thus, it is likely that these two reaction series are two different manifestations of a similar chemical step. Furthermore, the intrinsic entropy parameter $Ts_o^‡$ was more negative in uncoupled catalysis (−57.0 and −82.2 kJ/mol for coupled and uncoupled catalysis, respectively), indicating that formation of the transition state in uncoupled catalysis is more difficult to achieve and requires more structural constraints than in the case of coupled catalysis (*37*). These entropic effects were expected from the anticipation that coupled catalysis would involve the formation and breakage of more bonds than uncoupled catalysis as well as the influence of the transport mechanism in F_O.

The point on the isokinetic plot for γM23K mutant ATP synthesis also falls on the regression line for F_OF_1 catalysis (Figure 5). This indicates that the overall mechanism of cooperative ATP synthesis by the γM23K F_OF_1 (when ATP is made via the normal pathway) was the same as wild-type F_OF_1. Furthermore, the mutant enzyme apparently had a reasonably fast turnover for ATP synthesis similar to wild-type (Table 2) when ATP is made. The K_M for ADP and K_I for back inhibition by ATP were unchanged from wild-type values (Table 1). Clearly, the major difference was the almost 7-fold increase in the $K_{0.5}$ for P_i as well as the loss of cooperative interaction in the activation of ATP synthesis by P_i. These results are consistent with our finding that the off-rate constant for P_i is 49-fold increased relative to wild-type as determined in unisite conditions (*21*). The higher $K_{0.5}$ for P_i explains why relatively little ATP is synthesized at physiological concentrations of P_i (∼5 mM) and why the γM23K uncoupled enzyme could still synthesize net ATP (*18*, *20*). We reiterate that the γM23K mutation does not "uncouple" the enzyme in the same way as separation of F_1 from F_O; instead, the enzyme is inefficiently coupled (*20*). In other words, the transport and catalytic mechanisms are still communicating, but the mutation creates a slip or branched pathway through which the energy derived from the $\Delta\mu_H+$ or ATP hydrolysis is dissipated as heat (see below). The temperature dependence of the γM23K coupling efficiency (*38*) is thought to represent an increase of the rate of the uncoupled branch pathway as well as an increased proportion of the enzyme taking the branched pathway as a function of temperature.

The branched pathway affects the catalytic cycle primarily at the binding of P_i. (1) The affinity for P_i is lowered (Figure 1 and Table 1) due to an enhanced rate of P_i release (*21*), indicating that the enzyme is caught in a P_i release mode. (2) The communication between the two P_i binding β subunits is lowered as indicated by the lowered apparent P_i cooperativity (Figure 1 and Table 1). (3) There is a loss of nucleotide binding energy utilization (*21*) required for the efficient chemical synthesis of ATP. (4) There is an increase in interaction energy between γ and β subunits that needs to be overcome to achieve ATP hydrolysis (*18*) or synthesis (Table 2). Each of these effects suggests that the γM23K mutation perturbs the ability of the enzyme to obtain the exact conformation for P_i binding and causes an increased activation barrier that must be overcome to achieve the transition state for binding P_i.

Catalytic Pathway through Three Interacting Sites and Rotational Catalysis. With the kinetic and thermodynamic information on the effects of γM23K, we can update the model for ATP synthesis to reflect the role of energy coupling in the kinetic pathway. Furthermore, other recently reported information is important for the model. The crystallographic structure of Abrahams *et al*. (*7*) found three different nucleotide sites: the two ADP and P_i binding β subunits are not identical (presumably β_{DP} and β_E) and ATP is bound (and synthesized) on another conformation (β_{TP}). Some recent publications have speculated that the crystallographic structure of Abrahams *et al*. (*7*) is of an ADP inhibited state of F_1 (reviewed in ref 39). However, Löbau *et al*. (*40*) demonstrated that this is likely not the case and that the X-ray crystallographic structure with three different nucleotide states of active sites represents a true ground state of the enzyme which just released ATP from site β_E.

The γ subunit is clearly required for establishing the conformational asymmetry of the three β subunits (*41*) along with Mg^{2+} (*42*−*44*). Yet, there is also communication between catalytic sites to allow each site to sense when the other is occupied such that activities are coordinated. In part, this communication is likely to involve the γ subunit. We report here the effect of the γM23K mutation on the apparent cooperativity of P_i activation of ATP synthesis. We have suggested that γM23K forms an ionized hydrogen bond with βGlu381 of the β^{380}DELSEED^{386} segment of β_{DP} (*18*), whereas the crystallographic structure indicates that residue γGln269 interacts with β_E (*7*). Using mutagenesis, we have shown that γMet23, γArg242, and βGlu381 physically interact (C. J. Ketchum, M. K. Al-Shawi, and R. K. Nakamoto, unpublished data) and mutations at residue γGln269 suppressed the kinetic, thermodynamic, and uncoupling effects of γM23K (*18*, *25*). Furthermore, β subunit mutations suppressed the effects of a frame-shift mutation near the end of the γ subunit (*45*). Taken together these results indicate that β_E and β_{DP} are in communication through γ. Additionally, Capaldi and co-workers (*44*, *46*) have used cross-links between cysteine mutations on different subunits to show that the catalytic state of the enzyme determines the position of the γ subunit. Further communication between active sites has been shown to occur through α subunits (*47*−*49*).

Recent evidence has suggested that cooperative catalysis generally requires full nucleotide occupancy of the three catalytic β nucleotide binding sites (*35*, *50*) and the predominant form of enzyme during turnover contains one MgATP and two MgADP in the catalytic sites (*35*). Our results are supportive of this notion in that the binding of P_i

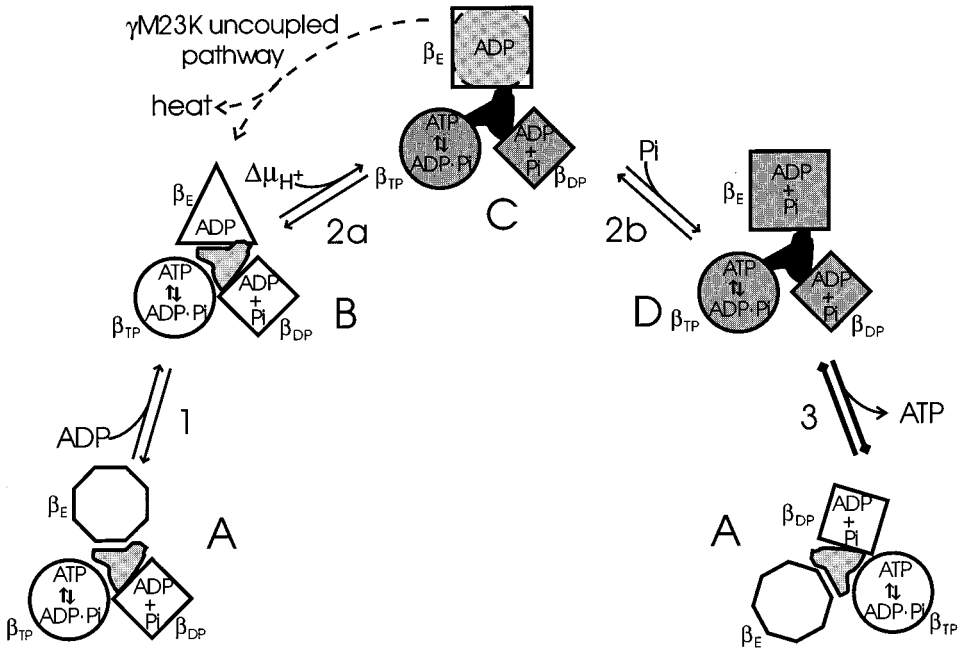

FIGURE 7: A model of the mechanism of F_OF_1-ATP synthase. This scheme shows the three catalytic sites, β_{TP}, β_{DP}, β_E, and the γ subunit (central figure) as seen in the crystallographic structure of Abrahams *et al.* (*7*). In the ground state (state A, left), ATP was previously synthesized at the first, high affinity site (β_{TP}, circle; ATP conformation) and is in reversible equilibrium with tightly bound ADP and P_i. β_{DP} (diamond) contains ADP and P_i bound in the ADP conformation. The asymmetrical γ subunit is shown interacting with the β_{DP} ^{380}DELSEED^{386} loop through the helical regions near residues γMet23 and γArg242 (γ18−35, γ238−246). Simultaneously, the helical region of the γ subunit surrounding residue γQ269 (γ269−280) interacts with β_E through the loop containing residue βT304. In step 1, ADP binds spontaneously to the empty site (β_E, hexagon, state A), which then isomerizes to an ADP binding conformation of state B (β_E, triangle). $\Delta\mu_H+$ energy is conformationally transferred to the whole F_OF_1 complex at step 2a leading to a destabilized high chemical potential form of the complex with occluded ADP (β_E, square; state C). Step 2a represents the coupling step and may involve a counter clockwise 60° rotation of the γ subunit (*44*). In state C, β_E has a much increased affinity for P_i, and P_i binding occurs spontaneously at step 2b yielding state D. Bound P_i triggers the relaxation of the high chemical potential form (step 3) to the ground state, low chemical potential form (state A, right), and realized energy drives the release of ATP from the high affinity site (β_{TP}) as well as the movement of γ subunit counter clockwise by the remaining 60°. Thus, step3 represents the power stroke of the binding energy change mechanism in which the γ subunit and nucleotide affinities of the three β subunits are rotated. ATP hydrolysis is the reverse of the above. The mutation γM23K leads to the formation of a ionized hydrogen bond with residue βGlu381 that holds the mutant complex in state C with a lowered affinity for P_i (β_E, rounded shaded square, state C). Occasionally, the γM23K complex in state C decays to state B by bypassing (dashed line) the coupling step 2a with the generation of heat in the absence of proton pumping (see Discussion for further details).

during ATP synthesis by wild-type enzyme appears to be cooperative, possibly indicating that two P_i and hence two ADP need to be bound before the enzyme relaxes to a ground state. Conversion to this ground state leads to the synthesis of a new ATP molecule at one of the two MgADP-occupied sites where the site adopts a high-affinity conformation and the concomitant release of one ATP, synthesized in the previous turnover, from the MgATP-occupied site. These results are consistent with and expand our previous binding energy change two-state model for ATP synthesis (*11*). In this model, two major active site conformations were considered, one for ATP binding ("unisite-like" conformation) and one for ADP binding.

Now, because of recent experimental evidence, the kinetic model must include rotational catalysis in which a minimum of the γ and ϵ subunits rotate relative to the $\alpha_3\beta_3$ hexamer and the turning movement drives each of the three catalytic sites through their cycles offset by 120° (*51*−*54*). From these results, our original model (*11*), and our new results, we generated a rotational catalysis binding energy change model of ATP synthesis (Figure 7). This model shares some features of previous models (*6*, *32*, *55*, *56*) but is different in that the steps and conformations required for energy conservation are explicitly indicated in terms of the known subunit structure and are hence amenable to further experimentation. Under physiological conditions, F_OF_1 ground state (Figure 7, state A) would have ATP bound to β_{TP} in the high affinity ATP binding conformation (Figure 7, circle) undergoing reversible hydrolysis/resynthesis. Binding of ADP to β_E would occur spontaneously (Figure 7, step 1) with an isomerization to the ADP binding conformation (Figure 7, triangle; see the preceding paper in this issue, ref 21). The energy from $\Delta\mu_H+$ is captured in the F_OF_1 complex in the form of conformational strain of the whole complex (Figure 7, step 2a) leading to a high chemical potential form of the enzyme (Figure 7, state C, β_E square). It is possible that movement of the γ subunit by 60° counterclockwise creates this strained conformation. State C or D is likely the intermediate captured by Grüber and Capaldi (*44*) by formation of a disulfide cross-link between αS411C and ϵS108C done in the presence of MgATP and $CuCl_2$. The high chemical potential state of the enzyme creates the P_i site in β_EADP (Figure 7, step 2b; see ref 11 for further details). The binding of P_i triggers the relaxation of the high chemical potential form of the enzyme (Figure 7, state D) to the ground state (Figure 7, state A, right) with the release of ATP from β_{TP} (Figure 7, step 3). Step 3 is the power stroke of the rotational binding energy change mechanism in which the γ subunit moves the remaining 60° counterclockwise leading to the changes in β subunit conformations and affinities such that β_{DP} becomes β_{TP}, β_{TP} becomes β_E, and β_E becomes β_{DP}, thus, regenerating the ground state (state

A) for the next turnover. Coupled ATP hydrolysis occurs by the reverse of above. The direction of catalytic rotation predicted by our model was recently verified experimentally (*54*). Thermodynamic analysis presented in this paper seems to implicate the rotational power stroke (step 3) as the rate-limiting step in coupled ATP synthesis and hydrolysis when the substrates were at saturating concentrations. The mutation γM23K leads to the formation of an ionized hydrogen bond with residue βE381 of β_{DP} that holds the mutant complex in state C with a lowered affinity for P_i (Figure 7, β_E, rounded shaded square, state C). Occasionally, the γM23K complex in state C decays to state B by bypassing (Figure 7, dashed line) the coupling step 2a with the generation of heat in the absence of proton pumping.

ACKNOWLEDGMENT

The authors thank Michelle L. Gonzales for excellent technical assistance.

REFERENCES

1. Penefsky, H. S., and Cross, R. L. (1991) *Adv. Enzymol. 64*, 173−213.
2. Capaldi, R. A., Aggeler, R., Turina, P., and Wilkens, S. (1994) *Trends Biol. Sci. 19*, 284−289.
3. Fillingame, R. H., Girvin, M. E., and Zhang, Y. (1995) *Biochem. Soc. Trans. 23*, 760−766.
4. Deckers-Hebestreit, G., and Altendorf, K. (1996) *Annu. Rev. Microbiol. 50*, 791−824.
5. Nakamoto, R. K. (1996) *J. Membr. Biol. 151*, 101−111.
6. Weber, J., and Senior, A. E. (1997) *Biochim. Biophys. Acta 1319*, 19−58.
7. Abrahams, J. P., Leslie, A. G. W., Lutter, R., and Walker, J. E. (1994) *Nature (London) 370*, 621−628.
8. Girvin, M. E., and Fillingame, R. H. (1993) *Biochemistry 32*, 12167−12177.
9. Wilkens, S., Dahlquist, F. W., McIntosh, L. P., Donaldson, L. W., and Capaldi, R. A. (1995) *Nat. Struct. Biol. 2*, 961−967.
10. Wilkens, S., Dunn, S. D., Chandler, J., Dahlquist, F. W., and Capaldi, R. A. (1997) *Nat. Struct. Biol. 4*, 198−201.
11. Al-Shawi, M. K., Parsonage, D., and Senior, A. E. (1990) *J. Biol. Chem. 265*, 4402−4410.
12. Al-Shawi, M. K., and Senior, A. E. (1992) *Biochemistry 31*, 878−885.
13. Gräber, P., and Labahn, A. (1992) *J. Bioenerg. Biomembr. 24*, 493−497.
14. Fischer, S., Etzold, C., Turina, P., Deckers-Hebestreit, G., and Altendorf, K. (1994) *Eur. J. Biochem. 225*, 167−172.
15. Souid, A.-K., and Penefsky, H. S. (1995) *J. Biol. Chem. 270*, 9074−9082.
16. Matsuno-Yagi, A., Yagi, T., and Hatefi, Y. (1985) *Proc. Natl. Acad. Sci. U.S.A. 82*, 7550−7554.
17. Penefsky, H. S. (1985) *Proc. Natl. Acad. Sci. U.S.A. 82*, 1589−1593.
18. Al-Shawi, M. K., Ketchum, C. J., and Nakamoto, R. K. (1997) *J. Biol. Chem. 272*, 2300−2306.
19. Inesi, G., Lewis, D., Nikic, D., Hussain, A., and Kirtley, M. E. (1992) *Adv. Enzymol. 65*, 185−215.
20. Shin, K., Nakamoto, R. K., Maeda, M., and Futai, M. (1992) *J. Biol. Chem. 267*, 20835−20839.
21. Al-Shawi, M. K., and Nakamoto, R. K. (1997) *Biochemistry 36*, 12954−12960.
22. Iwamoto, A., Miki, J., Maeda, M., and Futai, M. (1990) *J. Biol. Chem. 265*, 5043−5048.
23. Futai, M., Sternweis, P. C., and Heppel, L. A. (1974) *Proc. Natl. Acad. Sci. U.S.A. 71*, 2725−2729.
24. Lowry, O. H., Rosebrough, N. J., Farr, A. C., and Randall, R. J. (1951) *J. Biol. Chem. 193*, 265−275.
25. Nakamoto, R. K., Al-Shawi, M. K., and Futai, M. (1995) *J. Biol. Chem. 270*, 14042−14046.
26. Lessler, M. A., and Brierley, G. P. (1969) *Methods Biochem. Analysis 17*, 1−30.
27. Fabiato, A., and Fabiato, F. (1979) *J. Physiol. (Paris) 75*, 463−505.
28. Wise, J. G., and Senior, E. (1985) *Biochemistry 24*, 6949−6954.
29. Sugino, Y., and Miyoshi, Y. (1964) *J. Biol. Chem. 239*, 2360−2364.
30. Al-Shawi, M. K., and Senior, A. E. (1988) *J. Biol. Chem. 263*, 19640−19648.
31. Exner, O. (1973) *Prog. Phys. Org. Chem. 10*, 411−482.
32. Boyer, P. D. (1975) *FEBS Lett. 58*, 1−6.
33. Etzold, C., Deckers-Helestreit, G., and Altendorf, K. (1997) *Eur. J. Biochem. 243*, 336−343.
34. Hermolin, J., and Fillingame, R. H. (1989) *J. Biol. Chem. 264*, 3896−3903.
35. Weber, J., Bowman, C., and Senior, A. E. (1996) *J. Biol. Chem. 271*, 18711−18718.
36. Smékal, O., Reid, G. A., and Chapman, S. K. (1994) *Biochem. J. 297*, 647−652.
37. Cornish-Bowden, A. (1995) *Fundamentals of Enzyme Kinetics*, Portland Press, London.
38. Nakamoto, R. K., Maeda, M., and Futai, M. (1993) *J. Biol. Chem. 268*, 867−872.
39. Pedersen, P. L. (1996) *J. Bioenerg. Biomembr. 28*, 389−395.
40. Löbau, S., Weber, J., and Senior, A. E. (1997) *FEBS Lett. 404*, 15−18.
41. Kaibara, C., Matsui, T., Hisabori, T., and Yoshida, M. (1996) *J. Biol. Chem. 271*, 2433−2438.
42. Senior, A. E., Weber, J., and Al-Shawi, M. K. (1995) *Biochem. Soc. Trans. 23*, 747−752.
43. Grüber, G., and Capaldi, R. A. (1996) *Biochemistry 35*, 3875−3879.
44. Grüber, G., and Capaldi, R. A. (1996) *J. Biol. Chem. 271*, 32623−32628.
45. Jeanteur-De Beukelaer, C., Omote, H., Iwamoto-Kihara, A., Maeda, M., and Futai, M. (1995) *J. Biol. Chem. 270*, 22850−22854.
46. Aggeler, R., and Capaldi, R. A. (1996) *J. Biol. Chem. 271*, 13888−13891.
47. Maggio, M. B., Pagan, J., Parsonage, D., Hatch, L., and Senior, A. E. (1987) *J. Biol. Chem. 262*, 8981−8984.
48. Soga, S., Noumi, T., Takeyama, M., Maeda, M., and Futai, M. (1989) *Arch. Biochem. Biophys. 268*, 643−648.
49. Lee, R. S.-F., Wilke-Mounts, S., and Senior, A. E. (1992) *Arch. Biochem. Biophys. 297*, 334−339.
50. Weber, J., Wilke-Mounts, S., Lee, R. S.-F., Grell, E., and Senior, A. E. (1993) *J. Biol. Chem. 268*, 20126−20133.
51. Duncan, T. M., Bulygin, V. V., Zhou, Y., Hutcheon, M. L., and Cross, R. L. (1995) *Proc. Natl. Acad. Sci. U.S.A. 92*, 10964−10968.
52. Zhou, Y., Duncan, T. M., Bulygin, V. V., Hutcheon, M. L., and Cross, R. L. (1996) *Biochim. Biophys. Acta 1275*, 96−100.
53. Sabbert, D., Engelbrecht, S., and Junge, W. (1996) *Nature (London) 381*, 623−625.
54. Noji, H., Yasuda, R., Yoshida, M., and Kinosita, K. (1997) *Nature (London) 386*, 299−302.
55. Boyer, P. D. (1993) *Biochim. Biophys. Acta 1140*, 215−250.
56. Cross, R. L. (1981) *Annu. Rev. Biochem. 50*, 681−714.
57. Calhoun, M. W., Oden, K. L., Gennis, R. B., Mattos, M. J. T., and Neijssel, O. M. (1993) *J. Bacteriol. 175*, 3020−3025.
58. Hertzberg, E. L., and Hinkle, P. C. (1974) *Biochem. Biophys. Res. Commun. 58*, 178−184.

BI971478R